Positron scattering from pyrazine

Positron scattering from pyrazine

D. Edwards,[1] D. Stevens,[1] Z. Cheong,[1] V. Graves,[2] J. D. Gorfinkiel,[2] F. Blanco,[3] G. Garcia,[4] M. J. Brunger,[5,6] R. D. White,[7] and J. P. Sullivan[1]

[1]*Laser Physics Centre, Research School of Physics, Australian National University, 2601 Canberra, Australia*
[2]*School of Physical Sciences, The Open University, Walton Hall, MK7 6AA Milton Keynes, United Kingdom*
[3]*Departamento de Estructura de la Materia, Fisica Termica y Electronica e IPARCOS, Universidad Complutense de Madrid, 28040 Madrid, Spain*
[4]*Instituto de Fısica Fundamental, Consejo Superior de Investigaciones Cientificas, Serrano 113-bis, 28006 Madrid, Spain*
[5]*College of Science and Engineering, Flinders University, Adelaide, 5042 South Australia, Australia*
[6]*Department of Actuarial Science and Applied Statistics, Faculty of Business and Management, UCSI University, Kuala Lumpur 56000, Malaysia*
[7]*College of Science and Engineering, James Cook University, Townsville, 4810 Queensland, Australia*

(Received 11 July 2021; accepted 24 September 2021; published 12 October 2021)

The present paper provides a joint experimental and theoretical study of positron scattering from pyrazine. Experimental data were measured employing a low-energy positron beamline, and covered an energy range from 1 to 79 eV. Cross sections were measured for total scattering, total elastic scattering, positronium formation, direct ionization, and the sum of the total discrete electronic-state excitation processes. In addition, measured total electronic excitation cross sections for the individual 1^1B_{3u}, 1^1B_{2u}, 1^1B_{1u}, and 2^1B_{2u} states are also reported. Finally, experimental elastic differential cross sections (DCSs), here in the energy range 1–20 eV, are also presented. Results from two theoretical approaches are given: the *R*-matrix approach and the independent atom method with screening corrected additivity rule and interference terms. Where a comparison between our experimental and theoretical results could be made, the level of accord varied from being quite good to marginal depending on the actual scattering process under consideration. Last, a comparison between the present elastic DCS results and those from our earlier study on positron scattering from pyrimidine [Palihawadana *et al.*, Phys. Rev. A **88**, 012717 (2013)] showed a somewhat unexpected level of agreement.

DOI: 10.1103/PhysRevA.104.042807

I. INTRODUCTION

Positron emission tomography (PET) imaging remains the most sensitive and quantitative tomographic technique for imaging molecular interactions and pathways within the human body [1]. Early research machines of the 1960s have evolved rapidly into modern combination PET/CT (computerized tomography) scanners and, in the last few years, a total body PET machine has been produced which is capable of performing scans in under a minute [2]. The technical improvements of these machines have driven their research and clinical uses. PET scanners are now used for brain studies [3], cardiology [4], and oncology [5]. Positherapy [6] and theranostics [7] are also emerging fields which use *in vivo* positron emitting radioisotopes. However, there currently exists reluctance in the health care industry in the use of ionizing radiation in the general population, especially in the young or pregnant, which effectively prevents PET from reaching its full usefulness [5]. It is therefore imperative that a detailed understanding of the interactions of positrons with biological matter exists, in order to provide a quantitative description of the damage that these key diagnostic and therapeutic techniques produce within the human body.

While research into the scattering processes of low-energy positrons with biological targets has been ongoing for many years [8], it has largely been at the total cross section (TCS) level. These TCS measurements have failed to elucidate key details of the different scattering interactions, which provide a crucial test of the validity of scattering models for positrons in biological matter. The situation in regard to electron scattering is, however, much better [9,10], due in large part to the relative ease of generating high resolution electron beams. In order to fully model the path of positrons emitted in the body, along with liberated secondary electrons, Monte Carlo simulations have been used [11]. These simulations rely on accurate cross sections for a variety of biological molecules. Several models exist to calculate positron-molecule cross sections and it is one aim of the present work to provide experimental data to validate and help guide the development of these models.

Of the five primary nucleobases found in DNA and RNA, cytosine, uracil, and thymine are derived from pyrimidine. Pyrimidine itself is an aza-derivative of benzene whereby two CH groups (at positions 1 and 3 in the ring) are substituted for N atoms and this target has previously been the subject of positron scattering studies (e.g., [12]). Pyrazine, another aza-derivative of benzene, with two N atoms substituted at

ring positions 1 and 4, is an isomer of pyrimidine. Pyrazine is an interesting and potentially instructive target for cross section measurements and calculations because while similar in its physiochemical nature to pyrimidine (with isotropic dipole polarizabilities of ∼60 a.u. [13] and ∼59.3 a.u. [14] respectively), pyrimidine has a permanent dipole moment (∼2.33 D [15]) while pyrazine does not. Note that the NIST database [13] provides an extensive list of isotropic dipole polarizabilities for pyrazine, with those values depending on the quality of the model chemistry and basis functions employed in the various available computations. Here, we selected a value from one of the higher-level calculations in their table. The elastic integral cross section (ICS) and elastic differential cross sections (DCS) for positrons scattering from pyrazine have recently been calculated by Moreira and Bettega [16] using the Schwinger multichannel (SMC) method [17], for energies up to 10 eV. At the time of that publication there was no other theoretical work, or experimental data, available for direct comparison.

In contrast to the scarcity of available work concerning positron scattering, there have been several studies of electron scattering from pyrazine. Winstead and McKoy [18,19] used the SMC method to calculate the elastic ICS and elastic DCS at several energies, while the *R*-matrix method [20] has also been employed by Mašín and Gorfinkiel [21] to calculate inelastic and elastic cross sections. Palihawadana *et al.* [22], using the relative flow technique, measured elastic scattering cross sections and made a comparison to the above calculations where, generally, good quantitative agreement was found. Finally, the measurements and calculations of the total cross sections of Sanz *et al.* demonstrated similarly excellent agreement between the two [23], as well as with the *R*-matrix results previously mentioned [21]. A key result from investigations of electron scattering is the close similarity of the scattering cross sections for pyrazine and pyrimidine, at both the integral and differential cross section level, for energies above about 10 eV [12,22–24]. This suggests that the key driver of the collision dynamics is the molecular structure and dipole polarizability, with the dipole moment playing a lesser role which is virtually indiscernible at all but the lowest energies investigated in the previous studies. Another aim of the current work is to explore whether this behavior will also be found in the examination of positron scattering.

In this paper, we report on measurements and calculations of positron scattering from the pyrazine molecule. Experimental data include TCS and Ps formation cross sections in the energy range 1–79 eV. In addition, elastic DCS have also been measured at scattering energies between 1 and 20 eV. We also report the elastic and total inelastic (including electronic excitation and ionization) cross sections up to 20 eV along with the cross sections of four state resolved electronic excitations (1^1B_{3u}, 1^1B_{2u}, 1^1B_{1u}, and 2^1B_{2u}). All of these measurements were performed using the Australian Positron Beamline Facility [25], which delivers a pulsed positron beam with a full width at half maximum (FWHM) energy resolution of ∼55 meV in the present case. The experimental results are compared to cross sections calculated, also as a part of this study, using the independent atom model with screening corrected additivity rule and interference terms (IAM-SCAR+I) theoretical approach as well as the *R*-matrix method. Comparison is also made, where possible, to the previously published SMC calculation results [16].

II. EXPERIMENTAL METHODS

The experimental apparatus used for this work has been described in detail previously [25] so only a brief description will be given here. A 17-mCi ^{22}Na source in a sealed capsule was used to produce high energy positrons. This source capsule was cooled down to ∼7 K to facilitate the growth of a solid neon moderator which, through internal collisions, reduces both the energy and energy spread of the incident positrons. These slow positrons were then directed into a two stage buffer gas Surko trap. Inelastic collisions with a background gas mixture, containing N_2 and CF_4, trap and cool the incident low energy positron beam. Ejection from the trap was achieved by raising the bottom of the confining well over a defined potential, which sets the kinetic energy of the positron pulse. For the experiments presented here the trap was operated at 165 Hz and produced a monoenergetic pulsed beam with an energy width of 55 meV (FWHM). The ejected positrons were guided into the target stage by a 530-G solenoidal magnetic field. Positrons which undergo scattering with the buffer and cooling gases, post-trap ejection, are rejected by an initial retarding potential analyzer (RPA) before entering a 50-mm-long scattering cell. Pyrazine is a solid at room temperature, but has a sufficiently high vapor pressure, through sublimation, to provide a source of molecules for the collision experiments. A sample of high-purity ($\geqslant$99%) pyrazine was connected to the scattering cell via a manual needle valve, which was used to regulate pressure of the resulting vapor inside the scattering cell to keep the positron collision probability to below 10% in order to reduce the probability of multiple scattering events. The pressure inside the scattering cell was monitored using a temperature regulated, model 690 MKS Baratron capacitance manometer, which has a full range of 1 torr and a measurement accuracy of 0.05% at the typical pressures used in this work.

Analysis of the scattered positron beam takes place in a separate stage of the apparatus in a uniform magnetic field produced by another solenoid. A second RPA was used to measure the parallel energy distribution of the beam, in combination with a microchannel plate assembly. The strength of the magnetic field in this analysis stage can be varied to enable positrons which have lost parallel energy via inelastic or elastic collisions to be differentiated using the techniques described by Sullivan *et al.* [26]. These techniques, along with knowledge of the target number density inside the scattering cell, provide the means to measure the absolute cross sections at a given scattering energy. For elastic scattering, the angular resolution of the experiment, which occurs as a direct result of the finite energy resolution of the incident positron beam [27], must be taken into account as some portion of the scattered positrons will be unable to be distinguished from the primary beam [27]. Any comparison to the measured cross sections must account for this missing forward angle component, with the relevant missing angles for this work presented in Table I. It is also worth noting that any positrons that are elastically backscattered (scattered through an angle >90°) will be transported back towards the positron trap where they will

TABLE I. Missing angular range in the present experiment.

Energy (eV)	$\theta_{\min}$ (deg)	Correction (%)
1	13.7	23.7
5	6.1	30.3
10	4.3	20
20	3	12.4
50	1.9	13.1
70	1.6	15.4

be reflected from the potential of the final electrode. These reflected positrons will then pass back through the gas cell for a second time, where the majority will not undergo a second collision. This, therefore, will mean that any DCS measurement will be of the full angular range DCS "folded" about 90° [26], with the data presented over an angular range 0–90°. A consequence of the energy resolution for the experiments presented here is that vibrational and rotational excitations are unable to be effectively resolved for the positron scattering process, and so the cross sections presented here are averaged over the relevant rovibrational excitations.

III. THEORETICAL METHODS

A. Independent atom model with screening corrected additivity rule and interference terms

The independent atom model with screening corrected additivity rule (IAM-SCAR+I), has been applied in the same framework as our recent publication on positron scattering from furan [28], and as such only a brief description is presented here. This model has been successfully applied to positron scattering from several large molecules (see, for instance, Refs. [28,29]), for incident energies from 10 to 10 000 eV. The IAM-SCAR+I essentially treats the molecule as the sum of its constituent atoms, with scattering cross sections calculated using the optical potential method [30]. The atomic scattering potential can be represented by

$$V(r) = V_s(r) + V_p(r) - iV_a(r). \tag{1}$$

The real part of Eq. (1) drives the elastic scattering dynamics and includes the electrostatic $[V_s(r)]$ and polarization $[V_p(r)]$ interactions. The imaginary part $[V_a(r)]$ describes all inelastic processes that are considered as absorptions from the incident positron beam. Owing to this last term in Eq. (1), the optical model potential method yields a complex phase shift $\delta_l = \lambda_l + i\mu_l$. This allows for the calculation of the atomic scattering amplitudes, from which the corresponding differential and integral elastic as well as the integral inelastic and therefore the total cross sections are derived.

The calculations presented here also incorporate the consideration of interference effects [31]. This version of the theory is known as IAM-SCAR+I and basically provides the molecular differential cross section $(d\sigma^{\text{elastic}}_{\text{molecule}}/d\Omega)$ as a combination of the multicenter atomic amplitudes

$$\frac{d\sigma^{\text{elastic}}_{\text{molecule}}}{d\Omega} = \sum_{ij} f_i(\theta) f_j^*(\theta) \frac{\sin qr_{ij}}{qr_{ij}} \tag{2}$$

$$= \sum_{i} |f_i(\theta)|^2 + \sum_{i \neq j} f_i(\theta) f_j^*(\theta) \frac{\sin qr_{ij}}{qr_{ij}}. \tag{3}$$

Here the interference term is the second summation in Eq. (3). In this case $q \equiv |\vec{q}| = 2k \sin(\theta/2)$ is the momentum transfer and r_{ij} is the distance between atoms i and j.

Integration of the DCS allows for the calculation of the molecular integral cross sections, and the above techniques have the effect of extending the range of validity of the IAM method to well below 100 eV [30]. Including interference terms in the calculation of both integral and differential cross sections for molecular targets eliminates an earlier inconsistency between the differential and integral cross section values which is inherent to the IAM-SCAR method [32]. This means that no additional normalization procedure is required by the IAM-SCAR+I approach in order to fulfill the optical theorem.

B. *R* matrix

The *R*-matrix method and its computational implementations to model low energy electron and positron scattering from molecules are well established [33]. They have been extensively applied to electron collisions but significantly less so to positron scattering. This is due to two issues: (i) the implementations cannot model positronium formation; (ii) due to the lack of an exchange interaction, the accurate description of polarization effects is even more important for this projectile [34,35]. These two issues are particularly significant in the case of biologically relevant molecules that normally have low ionization thresholds (and therefore low positronium formation thresholds) and high dipole polarizabilities.

The details of the method have been described elsewhere [20,33]. We briefly summarize the approach as applied to the calculations in this work, within the fixed-nuclei approximation. Scattering calculations can be performed at different levels of approximation: here we have employed the static plus polarization (SP) model that involves modeling only the ground electronic state of the target and can therefore only describe elastic scattering.

The *R*-matrix method is based on the division of space into an inner and outer region, separated by a sphere of radius a; this radius is chosen so that the charge densities of all target electronic states of interest [as well as the $(N+1)$-electron configurations χ_i, see below] are negligible in the outer region. In the inner region, correlation effects between the positron and target electrons must be taken into account. In the outer region, these effects can be neglected. In the inner region, the set of basis functions Ψ_k^{N+1} that describe the target plus positron, i.e., the $(N+1)$-particle system, are expanded as follows within the SP model:

$$\Psi_k^{N+1} = \sum_{j=1}^{n_c} \Phi_{g.s.}(\mathbf{x}_N; \hat{r}_{N+1}; \sigma_{N+1}) \frac{u_j(r_{N+1})}{r_{N+1}} a_{jk} \times \sum_{i=1}^{m} \chi_i(\mathbf{x}_{N+1}) b_{ik}, \tag{4}$$

where $\mathbf{x}_N$ and $\mathbf{x}_{N+1}$ stand for the space and spin coordinates of all $N/N+1$ leptons, respectively. σ_{N+1}, r_{N+1}, and $\hat{r}_{N+1}$ stand for the spin, radial, and angular coordinates of the positron. The wave function $\Phi_{\text{g.s.}}$ describes the ground electronic state of the (N electron) target together with the angular and spin behavior of the positron. The functions

$\frac{u_j(r_{N+1})}{r_{N+1}}$ describe the radial part of the wave function of the positron. The L^2-integrable functions χ_i, built from bound target orbitals, both those occupied in the ground state configuration and virtual orbitals (VOs), describe the short-range polarization-correlation effects. The coefficients a_{jk} and b_{ik} are determined by diagonalizing the nonrelativistic Hermitian $(N+1)$ Hamiltonian in the inner region [20]. In the SP model, $\Phi_{\text{g.s.}}$ is calculated at the Hartree-Fock (HF) level; the L^2 configurations correspond to (i) configurations in which the positron occupies one of the orbitals in the ground state HF configuration; (ii) single excitations from said configuration (normally the core orbitals are kept frozen) into a set of VOs and the positron can occupy either bound or VOs.

In the outer region, the interaction between the positron and the target molecule is approximated by a single-center multiple expansion potential. The basis functions Ψ_k^{N+1} are used to construct the R matrix at the boundary between the regions. Propagation of the R matrix to an asymptotic distance and matching with known asymptotic expressions allows the K matrix to be determined. A trivial transformation provides the T matrices from which integral and angular DCSs can be calculated.

We have used the UKRmol suite [36] to determine T matrices and integral cross sections and the DCS code [37] to calculate the DCSs. We used the 6-311+G(3df,3pd) basis set and HF orbitals to describe the target. An R-matrix radius of $18a_0$ was required and partial waves up to $l = 4$ used; to build the L^2 functions, 120 VOs were used (these were not the lowest energy orbitals; those with amplitudes deemed too big at the boundary between regions were excluded). Tests were performed for different basis sets (more compact and more diffuse), different numbers of VOs and partial waves. The results presented here are the best we obtained. As indicated above, neither electronic excitation or positronium formation are modeled in these calculations. We also note that, when the SP approximation is used, pseudoresonances are visible in the integral cross sections [20]: these peaks are nonphysical and do not indicate the presence of resonances in the collision process. Pseudoresonances can be eliminated (or its number significantly reduced) in close-coupling (CC) calculations. To demonstrate this we also run a calculation using the 6-311+G** basis set, HF orbitals, the same R-matrix radius, 80 VOs to describe the L^2 functions, and partial waves up to $l = 5$ but where, instead of just the ground state, we included 80 target states generated from single excitations into the 80 VOs.

IV. RESULTS AND DISCUSSION

A. Grand total cross section

The data in Fig. 1 show the present experimental results for the grand total cross section, compared to the IAM-SCAR+I calculation. The figure presents both the full calculation as well as a version that is modified to allow for the limited angular resolution of the experiments, as described in Sec. II. For the correction, the theoretical total cross section is calculated for the integral of the DCS that corresponds to the limited angular range of measurement of the experiment. In particular, it excludes some portion of the forward scattering angles and

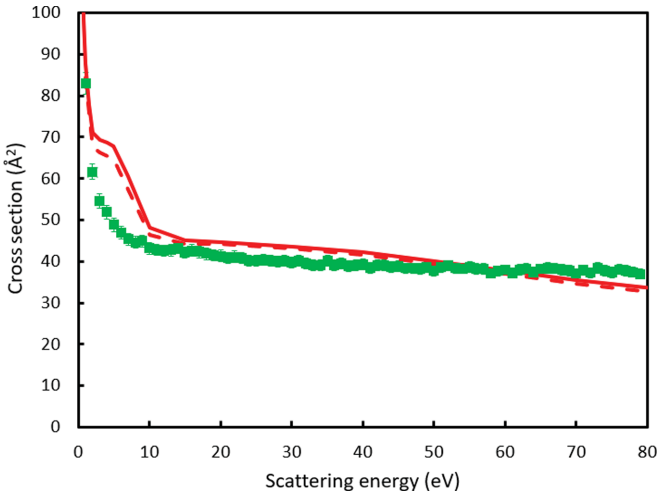

FIG. 1. The grand total cross section for positron scattering from pyrazine. The green squares are the experimental results. The red line is calculated from the IAM-SCAR+I method with the red dashed line being the same result but corrected for the missing angles.

provides a more relevant comparison to the experimental data. In general, the agreement between the measured values and the corrected IAM-SCAR+I data are quite good above 10 eV, although the dependence as a function of energy is somewhat different between the measurement and theory, and the two are not in strict agreement within the experimental error bars. The feature in the theoretical curve between 5 and 10 eV corresponds to the incorporation of positronium formation in the calculation, and is a consequence of the likely overestimation of this quantity in this energy range. This is explained further in the following section. The corrected version of the theory is only slightly lower in magnitude than the theory integrated over the full angular range. At the highest energies measured, there remains some disagreement across the energy range presented here, in contrast to previous work [12,28] which has typically seen better agreement as the incident energy increases. One key difference in this case is that there is no target permanent dipole moment, although the polarizability can still be a driving influence in the collision process. While the dipole moment is explicitly accounted for in the IAM-SCAR+I technique, polarizability arises as the sum of the constituent atomic polarizabilites, and is thus less likely to accurately reflect the true nature of the molecular interaction. In this case, it seems that this leads to the differences observed in the grand total cross section comparison here. Tabulated experimental data for the grand total cross section can be found in Table II.

B. Elastic scattering and positronium formation

The total elastic scattering cross sections are shown in Fig. 2, where the experimental results are compared to both the current theoretical calculations. To make an accurate comparison to the experimental data, comparison is also made to the appropriately modified calculations, integrated over the angular range of the experimental measurement, as previously described. In Fig. 3, we present the positronium formation cross section for pyrazine (experimental data for this cross

TABLE II. Experimental grand total (GTCS) and positronium formation (Ps) cross sections for positrons scattering from pyrazine (10^{-16} cm^2).

Energy (eV)	GTCS	Error	Ps	Error	Energy (eV)	GTCS	Error	Ps	Error
1	83.02	2.54	0.17	0.46	41	38.43	1.27	5.03	0.49
2	61.68	1.92	−0.17	0.47	42	39.02	1.28	4.12	0.49
3	54.67	1.72	1.41	0.47	43	39.05	1.29	4.79	0.49
4	51.89	1.65	4.84	0.48	44	38.62	1.27	4.13	0.48
5	48.82	1.56	5.88	0.51	45	38.90	1.29	4.14	0.50
6	46.91	1.51	6.17	0.48	46	38.33	1.27	4.51	0.50
7	45.32	1.45	6.59	0.48	47	38.36	1.27	4.66	0.49
8	44.63	1.43	7.18	0.48	48	38.21	1.26	4.01	0.50
9	44.94	1.45	6.30	0.49	49	38.68	1.28	4.20	0.50
10	43.15	1.39	6.66	0.48	50	37.73	1.26	3.14	0.49
11	42.82	1.39	7.75	0.50	51	38.54	1.27	4.30	0.51
12	42.60	1.38	7.25	0.49	52	38.98	1.29	3.29	0.50
13	42.76	1.39	6.77	0.49	53	38.34	1.27	3.58	0.51
14	43.23	1.40	7.32	0.49	54	38.31	1.26	3.63	0.49
15	42.18	1.37	7.80	0.49	55	38.62	1.28	3.32	0.48
16	42.63	1.38	7.90	0.50	56	38.22	1.26	3.41	0.51
17	42.26	1.37	7.65	0.49	57	38.16	1.26	3.42	0.49
18	41.82	1.36	7.69	0.48	58	37.16	1.24	3.76	0.50
19	41.46	1.35	8.04	0.48	59	37.72	1.25	3.19	0.51
20	41.35	1.35	7.83	0.49	60	37.89	1.26	2.79	0.50
21	40.89	1.34	7.31	0.48	61	37.22	1.23	2.68	0.49
22	41.13	1.34	7.21	0.49	62	38.04	1.26	2.99	0.51
23	40.91	1.34	6.67	0.49	63	38.27	1.26	2.98	0.50
24	40.07	1.31	6.76	0.48	64	37.35	1.24	2.39	0.50
25	40.17	1.31	7.38	0.49	65	38.12	1.27	2.60	0.49
26	40.33	1.32	6.54	0.50	66	38.38	1.27	2.63	0.51
27	40.16	1.31	6.84	0.49	67	38.28	1.27	2.57	0.49
28	40.03	1.31	6.15	0.47	68	37.93	1.26	2.32	0.50
29	40.26	1.32	6.54	0.51	69	37.75	1.25	2.19	0.50
30	39.81	1.31	6.15	0.51	70	37.07	1.23	2.44	0.50
31	40.23	1.32	6.67	0.49	71	37.92	1.25	2.66	0.51
32	39.58	1.30	5.10	0.48	72	37.27	1.24	2.35	0.50
33	39.12	1.29	5.73	0.50	73	38.37	1.27	2.97	0.50
34	39.09	1.28	5.73	0.48	74	37.74	1.25	2.95	0.50
35	40.27	1.32	5.07	0.49	75	37.35	1.24	2.54	0.50
36	39.10	1.29	5.26	0.49	76	38.06	1.26	2.28	0.50
37	39.48	1.30	5.28	0.50	77	37.79	1.24	2.61	0.50
38	38.89	1.28	5.27	0.49	78	37.40	1.24	2.31	0.50
39	39.01	1.29	5.81	0.50	79	36.95	1.24	2.24	0.50
40	39.32	1.30	4.60	0.51					

section are also given in Table II), comparing the experimental measurements to the phenomenological approach taken in the IAM-SCAR+I calculation.

As has been observed previously [28,29], there is general agreement between experiment and theory in terms of the shape and magnitude of the positronium formation cross section, with some discrepancy between the two thresholds. The onset of positronium formation in the IAM-SCAR+I model occurs more than 4 eV above the measured value—an expected result given that the threshold used in this theory is calculated based on the ionization potential of the constituent atoms, rather than the true molecular ionization threshold. The calculation underestimates the measured cross section throughout most of the energy range covered in Fig. 3, but shows better absolute agreement at higher energies. The energy of the peak in the calculation is a reasonable match to that of the measured cross section. While IAM-SCAR+I employs a phenomenological approach to calculate positronium formation, it is sufficient to reproduce the general details of the cross section, although it does appear to omit a certain level of detail, in particular regarding its absolute magnitude and near threshold behavior.

The influence of the positronium formation calculation can also be seen in the total elastic scattering cross section (shown in Fig. 2), which exhibits a "bump" corresponding to the calculated peak of the positronium formation cross section, where one might expect a smoothly decreasing cross section—as seen in the experimental measurements. The comparison between experiment and the IAM-SCAR+I theory for elastic scattering is reasonable at best, although it appears to be improving at the limits of the experimental data range. This may be anticipated, as this theoretical approach can be

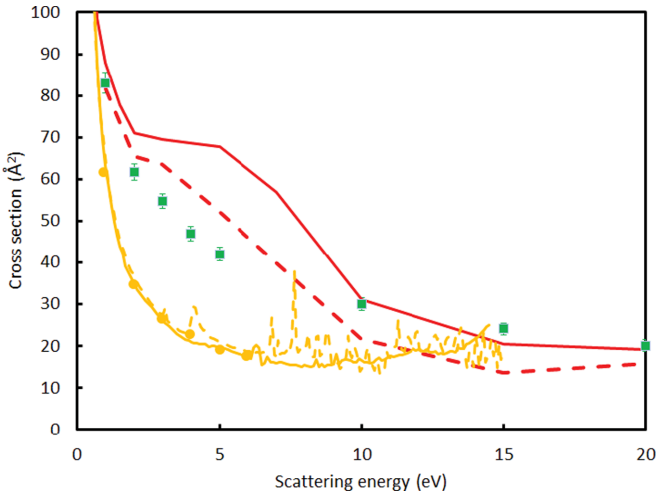

FIG. 2. Total elastic cross section for positrons interacting with pyrazine. The green squares are the present experimental results. The results of the IAM-SCAR+I calculation are plotted as the red line with the red dashed line being the same calculation corrected for the missing angles of the experiment. The yellow solid line is from the *R*-matrix CC calculation, with the yellow dashed line the *R*-matrix SP calculation, as described in the text in Sec. III B. The yellow circles are the *R*-matrix SP calculation corrected for the experimental angular range, at selected energies.

expected to have difficulty fully accounting for the physics of the interaction at low energies where molecular structure effects will be strongest. In the case of the *R*-matrix calculation, also shown in Fig. 2, the comparison between experiment and theory shows little agreement. In both theoretical cases, the effect of the limited experimental angular range on the modified calculations is not very large, due to a relatively small contribution from forward angle scattering. This is further explored in the following section. Note that the correction was only made for a selection of the energies calculated in the *R*-matrix case.

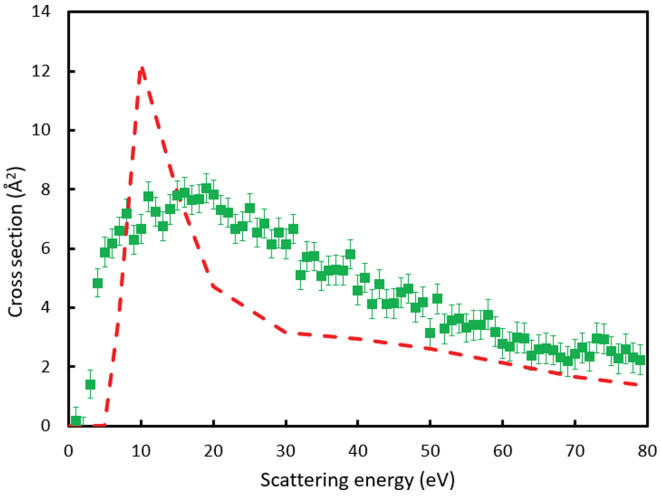

FIG. 3. Positronium formation cross section for pyrazine between 0 and 80 eV. The green squares are the present experimental data and the red dashed line is the result from the IAM-SCAR+I calculation.

The *R*-matrix theory shows evidence of many nonphysical pseudoresonances, in particular the SP model; the CC result is significantly smoother but both the cross sections are of very similar size and underestimate the experiment for all the energies calculated. The rapid increase of this cross section as the scattering energy approaches 0 eV is indicative, in nonpolar targets, of the presence of a virtual state. This increase is due to the ^2A_g contribution to the cross section. Moreira and Bettega estimated the scattering length from their eigenphase sum and obtained a positive value, which is consistent with the existence of a bound (rather than virtual) state [38]. A fit of our ^2A_g eigenphase at very low energy also returns a positive value for the scattering length: the modulus seems to be very sensitive to the energy range chosen for the fit, but it does indicate a state more weakly bound than the one characterized by Moreira and Bettega. We note that for both the IAM-SCAR+I and *R*-matrix calculations, the effect of the limited experimental angular range on the modified results is not very large, because in general the angular differential cross sections (see next section) are not very forward peaked; when this is the case, the difference in the integral cross section is more noticeable.

C. Elastic differential cross sections

Figure 4 shows the lowest energy DCS measurements and calculations at impact energies of 1–3 eV. Where data are available, comparisons have also been made to the SMC results of Moreira and Bettega [16], and the experimental data for positron scattering from pyrimidine [12]. All of the calculated results have been folded around 90°, as discussed in Sec. II, to allow for direct comparison to the experimental measurements. At 1 eV, the experimental data are much more strongly forward peaked than any of the calculations, although from (folded) scattering angles of approximately 30° and higher we see good agreement in the shape between experiment and the present *R*-matrix calculations, which are also very similar to the results of the SMC approach. There is, however, a significant difference in the magnitude of the cross section between experiment and theory across this angular range, outside the absolute error bars presented for the experimental data. The IAM-SCAR+I calculation at this energy is considerably flatter than the other two calculations, and is in poor agreement with the experimental data seen in Fig. 4(a). The data for positron scattering from pyrimidine are considerably more forward peaked at this energy, which may be expected due to the additional permanent dipole moment for that molecule, compared to the present target. At the more backwards angles, the two experimental cross sections are in agreement in both shape and magnitude.

At 2 and 3 eV, Figs. 4(b) and 4(c) respectively, the comparison to the *R*-matrix calculations and the SMC data is much the same as the case for 1 eV, with both in good agreement with the experimental data at scattering angles above about 30°. However, it does appear that these calculations miss the increasingly forward peaked nature of the DCS as the energy is increased. At these energies, the IAM-SCAR+I calculation is now more forward peaked and is qualitatively closer to the experimental result, although there is still significant disagreement across the entire angular range in both magnitude and

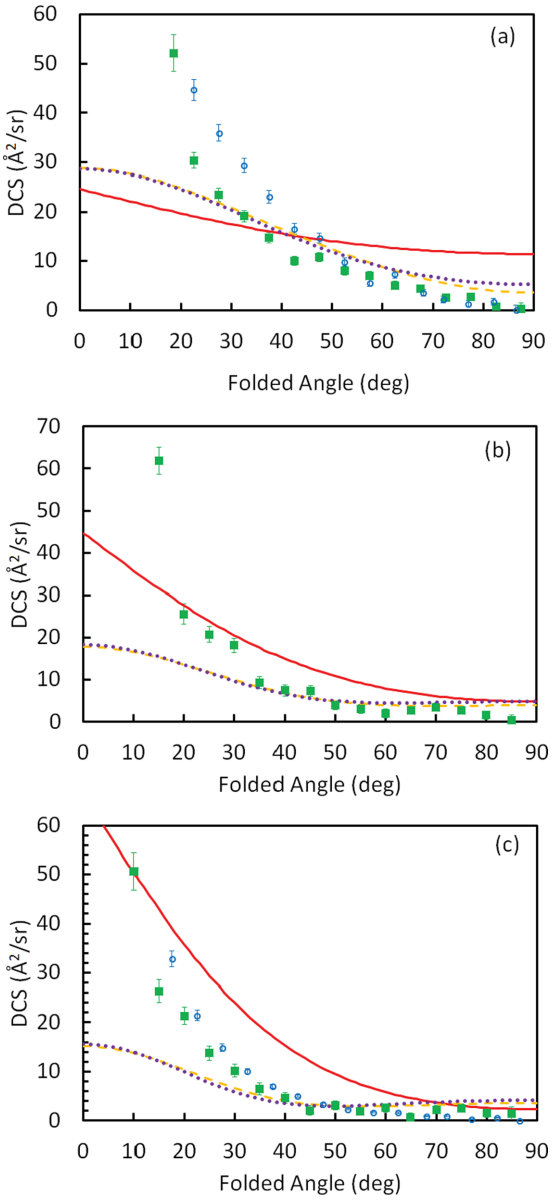

FIG. 4. Differential cross sections for positrons scattering from pyrazine at (a) 1 eV, (b) 2 eV, and (c) 3 eV. The green squares are the experimental values, the red lines are the results of the IAM-SCAR+I calculations, the yellow dashed lines are calculated with the *R*-matrix method at the SP level, and the purple dotted line is from the SMC calculation of Moreira and Bettega [16]. The blue circles are previous experimental data for positron scattering from pyrimidine [12].

shape. This is not entirely an unexpected result, as at these low impact energies, the approximations underlying the IAM-SCAR+I method are unlikely to be valid when considering scattering from a relatively complex molecule. The present experimental data are in closer agreement with the previous experiments for positron scattering from pyrimidine at 3 eV, in particular at angles less than about 40°. It does appear that the DCS is still more forward peaked in the case of pyrimidine, again, to be expected given the permanent dipole moment of the molecule.

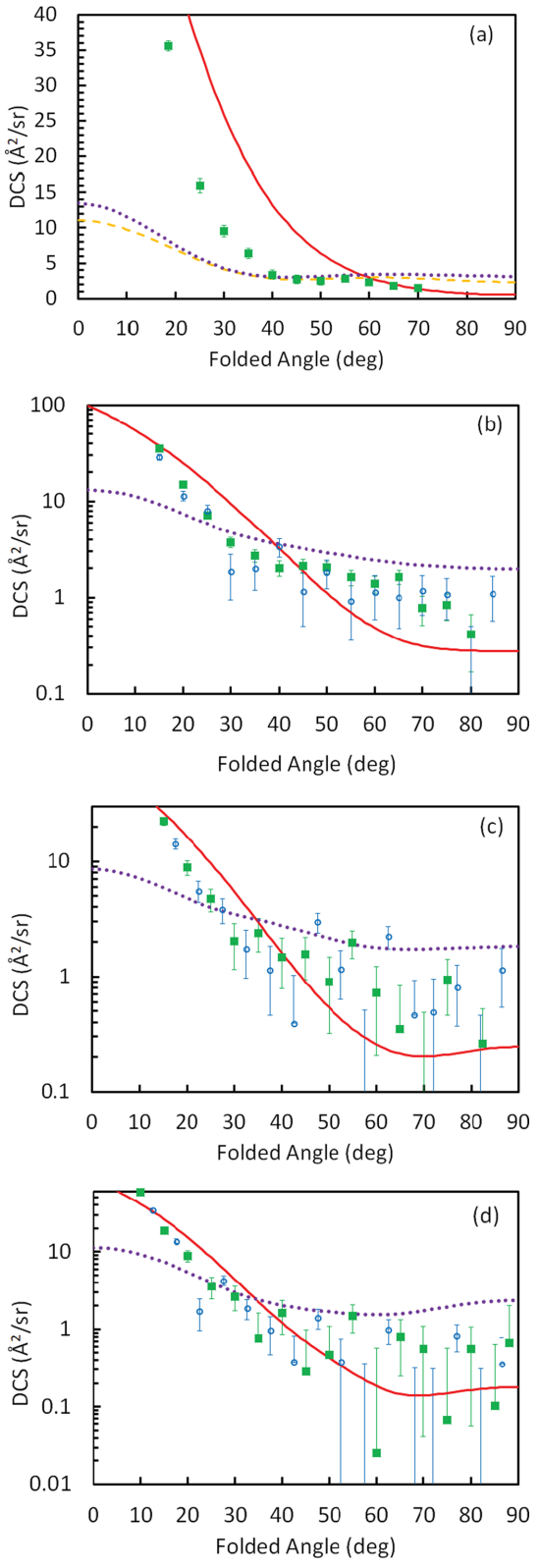

FIG. 5. Differential cross sections for positrons scattering from pyrazine at (a) 5 eV, (b) 10 eV, (c) 15 eV, and (d) 20 eV. The green squares are the experimental values, the red lines are the results of the IAM-SCAR+I calculations, the yellow dashed lines are calculated with the *R*-matrix method at the SP level, and the purple dotted line is from the SMC calculation of Ref. [16]. The blue circles are previous experimental positron cross sections for pyrimidine [12].

TABLE III. Experimental differential cross sections for positrons scattering elastically from pyrazine (10^{-16} cm^2 str^{-1}).

Angle	1 eV	Error	Angle	2 eV	Error	3 eV	Error	5 eV	Error	10 eV	Error	15 eV	Error	20 eV	Error
18.5	52.15	3.72	10.0			50.60	3.83							59.10	2.80
22.5	30.32	1.62	15.0	61.81	3.20	26.32	2.28			35.11	0.92	22.36	1.69	18.79	1.84
27.5	23.49	1.37	18.5					35.58	0.71						
32.5	19.10	1.19	20.0	25.56	2.41	21.36	1.79			14.95	0.70	8.81	1.27	8.83	1.41
37.5	14.76	1.06	25.0	20.81	1.94	13.74	1.50	15.95	1.01	7.19	0.57	4.70	1.05	3.59	1.12
42.5	10.04	0.96	30.0	18.14	1.66	10.21	1.31	9.53	0.85	3.76	0.49	2.02	0.88	2.65	0.94
47.5	10.73	0.90	35.0	9.35	1.45	6.48	1.17	6.40	0.73	2.73	0.43	2.40	0.77	0.76	0.84
52.5	7.96	0.84	40.0	7.50	1.31	4.70	1.08	3.37	0.69	2.03	0.38	1.46	0.68	1.60	0.74
57.5	7.02	0.79	45.0	7.36	1.22	2.09	0.97	2.72	0.61	2.13	0.34	1.57	0.62	0.28	0.69
62.5	5.06	0.77	50.0	3.98	1.11	3.08	0.91	2.49	0.56	2.07	0.32	0.90	0.58	0.47	0.63
67.5	4.35	0.75	55.0	3.04	1.07	1.95	0.87	2.83	0.52	1.62	0.29	1.96	0.54	1.49	0.59
72.5	2.49	0.73	60.0	2.04	1.02	2.62	0.84	2.28	0.48	1.39	0.28	0.72	0.51	0.03	0.55
77.5	2.66	0.77	65.0	2.76	0.98	0.71	0.82	1.80	0.47	1.65	0.27	0.35	0.49	0.79	0.55
82.5	0.65	0.85	70.0	3.52	0.98	2.25	0.80	1.46	0.46	0.77	0.26	0.00	0.49	0.56	0.52
87.5	0.21	1.22	75.0	2.75	0.98	2.55	0.84			0.83	0.25	0.94	0.48	0.07	0.51
			80.0	1.58	1.04	1.63	0.93			0.42	0.25			0.56	0.50
			82.5									0.26	0.26		
			85.0	0.36	1.25	1.47	1.36							0.10	0.54
			88.0											0.68	1.34

Data for the elastic DCS between 5 and 20 eV are shown in Fig. 5. At 5 eV, the discussion is very similar to that at 3 eV, although agreement between the experimental data and the calculation using the IAM-SCAR+I approach has again improved somewhat, as the theoretical cross section becomes more forward peaked. While there is still close agreement between the results of the *R*-matrix and SMC calculations, we see that the SMC data are now somewhat more forward peaked, although not to the same extent as the IAM-SCAR+I calculation or the experiment, as can be seen in Fig. 5(a). The DCS behavior above 40° is again well described by the *R*-matrix and SMC approaches, while large differences in the shape of the DCSs are still evident in the comparison with the IAM-SCAR+I calculation. As the energy increases up to 20 eV, shown in Figs. 5(b)–5(d), we see that the agreement between experiment and the IAM-SCAR+I calculation continues to improve, and that the experimental data for 10-eV scattering and above closely matches that for positron scattering from pyrimidine. At these energies, the SMC calculation continues to underestimate the forward scattering behavior and starts to predict a higher cross section than observed in the experiment at the larger scattering angles. This is likely due to the opening of electronic excitation and ionization channels, which are not explicitly included in the calculation and may be expected to have some effect on the elastic scattering process (such as through flux sharing). Conversely, as the details of the molecular structure become less critical in the scattering process we can see that the IAM-SCAR+I approach is able to much more closely reproduce the experimental data. Again, this might be expected due to the nature of the calculation and is in line with previous comparisons to other similar molecules in this energy range (e.g., Ref. [28]).

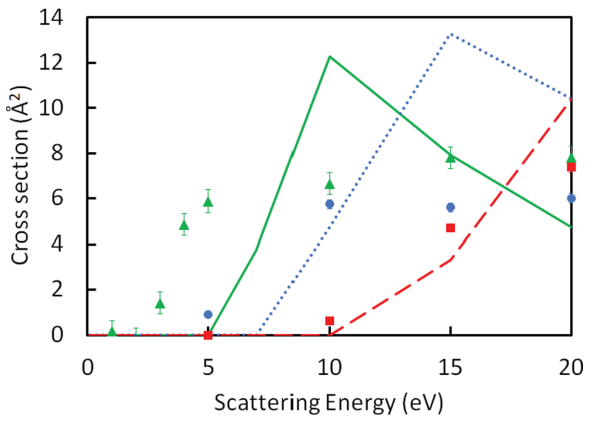

FIG. 6. Integral inelastic cross sections for positrons scattering from pyrazine. Ps formation in the green solid line (IAM-SCAR+I theory) and green triangles (experiment), total electronic excitation in the blue dotted line (IAM-SCAR+I theory) and blue circles (experiment), and ionization in the red dashed line (IAM-SCAR+I theory) and red squares (experiment)

In general, we see that the present *R*-matrix approach does a good job in the lower energy range, below 10 eV, in describing the observed experimental elastic scattering DCSs at angles greater than about 30°. However, it is not able to reproduce the forward angle scattering seen across the energy range presented here. This suggests that the structure models used failed to fully account for the polarization of pyrazine due to the presence of the positron. As explained previously, this issue is well known: tests were performed in an attempt to improve the description of these effects by inclusion of pseudocontinuum orbitals and pseudostates. Their use showed a clear improvement (increase in size) of forward angle cross sections for small molecules like C_2H_2 [35], but have not delivered cross sections for pyrazine close to experiment in magnitude. This could be due either to the size of the molecule or to the fact that its polarizability is more than twice that of C_2H_2. It is interesting, however, that agreement with the SCM results is, overall, excellent with the conclusion that both methods seem to be describing the scattering physics at the same level of detail. We also note the clearly better agreement,

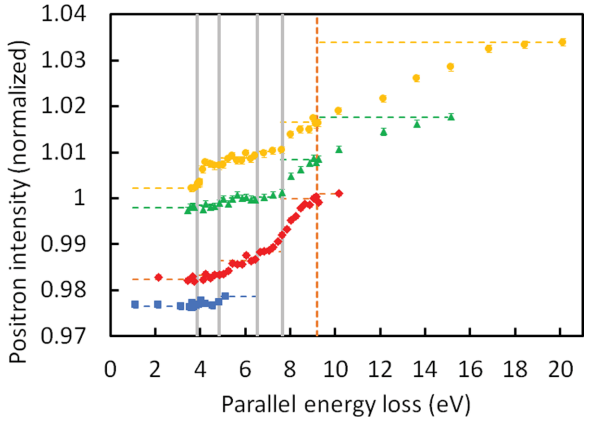

FIG. 7. Positron intensity as a function of energy loss. The different colored curves represent impact energies of 5, 10, 15, and 20 eV, from bottom to top. The curves have been offset for clarity, but relative intensity changes have been preserved. The thresholds for the excited states measured are shown by the grey lines, and steps can be clearly seen in the data, corresponding to the different state excitations. The ionization threshold is marked by the orange dashed vertical line.

at angles below 30°, between DCSs from *R*-matrix calculations and experiment for the polar molecule pyrimidine [12]. In that case, even though the calculations still underestimated the DCSs, the strong dipole effects (included by means of a Born correction) seemed to conceal any deficiencies in the description of target polarization.

Conversely, we see that agreement between experiment and the IAM-SCAR+I approach improves as the scattering energy increases, something that has been noted in previous work [12,28] and is likely due to the reduced impact of the details of the molecular structure on the scattering process as the impact energy increases. Despite the lack of a permanent dipole moment in pyrazine, the experimental data presented here are in close agreement with previous measurements of positron scattering from pyrimidine, with some differences for forward angle scattering at the lowest scattering energies. This suggests, similar to that observed in the corresponding electron scattering studies from both molecules [22], that it is the target polarizability that is dominating the elastic scattering dynamics above about 5 eV. Tabulated experimental data for the DCS measurements presented here can be found in Table III.

D. Inelastic scattering

For discrete energies in the range 5–20 eV, the experimental measurements were able to resolve discrete electronic excitation and ionization cross sections. Figure 6 shows the present experimental results for total (direct) ionization and total electronic excitation in this energy range, compared to the IAM-SCAR+I calculation, which accounts for inelastic processes using an absorption potential approach. The positronium formation cross section is also shown here, for reference. These three cross sections, combined with elastic scattering, represent the maximum degree of partitioning available using the IAM-SCAR+I approach, and we can see

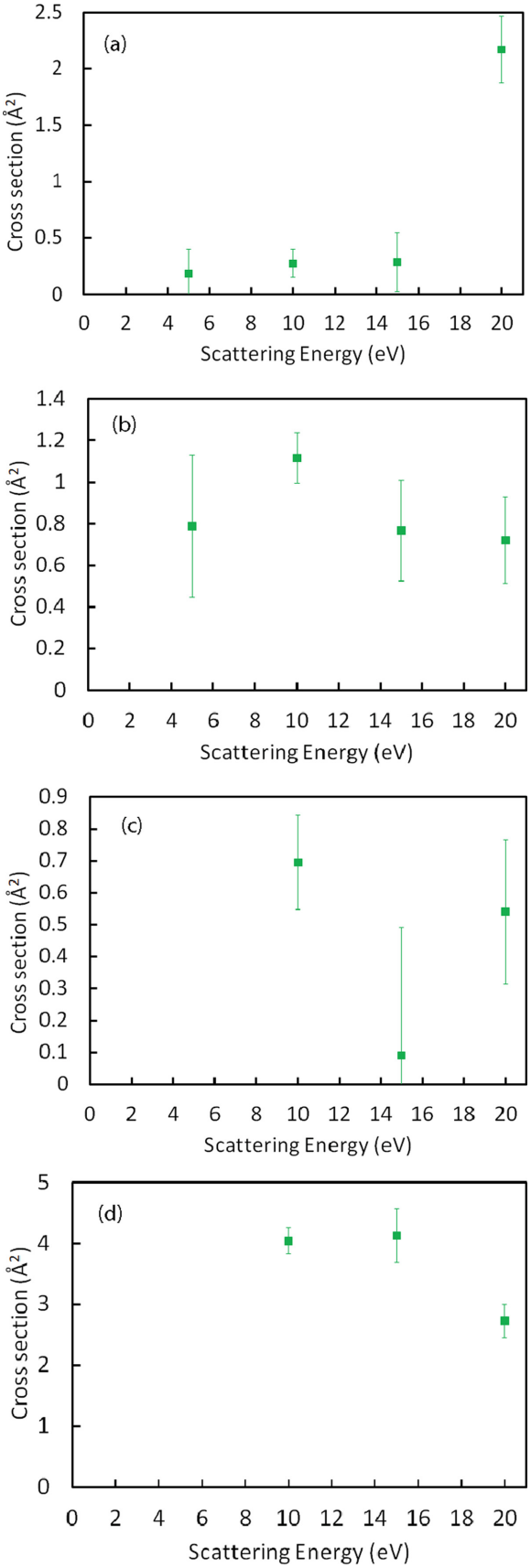

FIG. 8. Individual state-resolved experimental electronic excitation cross sections for pyrazine states (a) 1^1B_{3u}, (b) 1^1B_{2u}, (c) 1^1B_{1u}, and (d) 2^1B_{2u} at impact energies between 5 and 20 eV.

TABLE IV. Experimental total cross sections for positrons scattering elastically and inelastically from pyrazine (10^{-16} cm^2). The bottom section gives the measurements for the individual state-resolved cross sections.

Energy (eV)	Elastic	Error	Electronic ex.	Error	Ionization	Error		
1	83.02	2.54						
2	61.68	1.92						
3	54.67	1.72						
4	47.04	1.72						
5	42.05	1.64	0.90	0.03	0.00	0.00		
10	30.10	1.48	5.75	0.19	0.64	0.02		
15	24.09	1.47	5.60	0.19	4.68	0.16		
20	20.11	1.45	6.01	0.20	7.40	0.25		
	$1\,^1B_{3u}$	error	$1\,^1B_{2u}$	error	$1\,^1B_{1u}$	error	$2\,^1B_{2u}$	error
5	0.18	0.22	0.79	0.34				
10	0.27	0.12	1.12	0.12	0.70	0.15	4.04	0.21
15	0.29	0.26	0.77	0.24	0.09	0.40	4.13	0.44
20	2.17	0.30	0.72	0.21	0.54	0.23	2.73	0.27

that the comparison is good in this case, over the limited energy range available for the experimental data. Although there are some differences in magnitude and threshold energies between the cross sections, in general the partitioning appears to be in reasonably good agreement between experiment and theory, giving confidence in the theoretical results for higher energies. We present a direct comparison between experiment and theory at this level, with previous experiments (for instance [28]) unable to resolve excitation and ionization processes.

In fact, the present experiment was also able to measure the cross sections for individual electronic excitations of the pyrazine molecule. This took advantage of improved experimental operation which allowed for the application of the magnetic field ratio technique, as described in Sullivan *et al.* [26], and applied to positron scattering from several atoms and molecules [39–41], to resolve the excitations of the 1^1B_{3u}, 1^1B_{2u}, 1^1B_{1u}, and 2^1B_{2u} electronic states. The states and classifications were identified through their threshold energies, taken from Wadt *et al.* [42], and in the measurements here the four excitations can be clearly identified, as shown in Fig. 7. In this case, the possibility of excitation to tripletlike states was discounted, due to the fact that systems composed of relatively light atoms, such as the pyrazine molecule, can only populate those states from the singlet ground state through an exchange process. This is, of course, impossible in the case of positron scattering. By measuring the step heights associated with each threshold, as indicated in the figure, and normalizing appropriately, the cross sections are then able to be determined. These cross sections are shown in Fig. 8. The highest energy state, 2^1B_{2u}, has by far the largest cross section of the four excitations measured, peaking at around 4×10^{-16} cm^2. The lowest cross section is for the 1^1B_{3u} at approximately 0.3×10^{-16} cm^2. However, we do see that the magnitude of the 1^1B_{3u} excitation jumps significantly at 20 eV impact energy, something clearly reflected in the data shown in Fig. 7. The other cross sections have magnitudes around 1×10^{-16} cm^2 across the energy range sampled here. The experimental data for the inelastic scattering is presented in Table IV, along with the measured total elastic scattering cross section.

V. CONCLUSION

This paper has presented a comprehensive study of positron scattering from the pyrazine molecule, at energies up to 80 eV. Experimental measurements have been compared to two theories, the IAM-SCAR+I and *R*-matrix techniques, which take different approaches in their description of the scattering problem. Comparison was also made to previously published results using the SMC framework [16]. We can see that each theory has its own strengths and weaknesses in the calculation of the various scattering cross sections. At the lowest energies studied, the *R*-matrix calculations presented here were in good agreement with the experimental data for all but the most forward scattering angles. This is also true for the SMC calculations, although we note that the discrepancies at forward scattering angles led to disagreement in the magnitude of the total elastic scattering cross section. It appears that, even though the problem is simplified relative to the case of molecules with a permanent dipole moment, more work needs to be done to fully take into account the effects of the polarizability of the target in the collision process. This conclusion is borne out by comparison to previous experimental data for positron scattering from pyrimidine, which has a similar polarizability to pyrazine, but also has a significant permanent dipole moment. It is also consistent with previous observations of electron scattering from these targets. At the elastic DCS level, for the energies examined here, we see that the permanent dipole moment leads to some differences in how forward peaked the DCS becomes at the lowest scattering energies, but at energies of 10 eV and above, there is little to separate positron scattering from the two targets. The conclusion is that the low energy dynamics of the scattering process are driven by the dipole polarizability, which is similar for both targets. This is a somewhat unexpected result, a naive consideration may have expected the permanent dipole to lead to much greater differences in the scattering of positrons from the two targets. The IAM-SCAR+I approach has been used to calculate positron scattering from a wide variety of molecular targets, and can be seen to do a good job here for energies above about 10 eV. This is not only true for elastic scattering, but also for inelastic processes,

which are treated using the absorption potential approach. The partitioning between ionization and electronic excitation can be seen to be reasonable when compared to the experimental data, and the positronium formation cross section calculated using this approach is in line with expectations from previous comparisons between experiment and theory for a range of different molecules. At the lowest energies, where molecular structure can be expected to have the biggest effect on the scattering process, we see that the IAM-SCAR+I approach struggles to reproduce the experimental results.

Experimental data were also presented here for state-specific total electronic excitation cross sections. To date, there have been no calculations of these cross sections for positron scattering from this class of molecule. It is clear that there is still much work to do to resolve the finer details of positron interactions with even moderately complex targets, which will be required as the demand increases for higher quality input data into modeling processes.

ACKNOWLEDGMENTS

The authors would like to acknowledge R. Tranter for his ongoing technical support of the experimental apparatus used in these experiments. Funding is acknowledged from the Australian Research Council Discovery program (Grant No. DP190100696). V.G. acknowledges support from the EPSRC Doctoral Training Partnership EP/T518165/1. F.B. and G.G. acknowledge partial financial support from the Spanish Ministerio de Ciencia e Innovación (Project No. PID2019-104727RB-C21) and CSIC (Project No. LINKA20085).

[1] J. J. Vaquero and P. Kinahan, Annu. Rev. Biomed. Eng. **17**, 385 (2015).
[2] R. D. Badawi, H. Shi, P. Hu, S. Chen, T. Xu, P. M. Price, Y. Ding, B. A. Spencer, L. Nardo, W. Liu *et al.*, J. Nucl. Med. **60**, 299 (2019).
[3] T. Jones and E. A. Rabiner, J. Cereb. Blood Flow Metab. **32**, 1426 (2012).
[4] F. M. Bengel, T. Higuchi, M. S. Javadi, and R. Lautamäki, J. Am. Coll. Cardiol. **54**, 1 (2009).
[5] A. Gallamini, C. Zwarthoed, and A. Borra, Cancers **6**, 1821 (2014).
[6] R. M. Moadel, R. H. Weldon, E. B. Katz, P. Lu, J. Mani, M. Stahl, M. D. Blaufox, R. G. Pestell, M. J. Charron, and E. Dadachova, Cancer Res. **65**, 698 (2005).
[7] E. C. Dijkers, T. H. Oude Munnink, J. G. Kosterink, A. H. Brouwers, P. L. Jager, J. R. de Jong, G. A. van Dongen, C. P. Schröder, M. N. Lub-de Hooge, and E. G. de Vries, Clin. Pharmacol. Ther. **87**, 586 (2010).
[8] M. J. Brunger, S. J. Buckman, and K. Ratnavelu, J. Phys. Chem. Ref. Data **46**, 023102 (2017).
[9] M. J. Brunger, Int. Rev. Phys. Chem. **36**, 333 (2017).
[10] J. D. Gorfinkiel and S. Ptasińska, J. Phys. B: At. Mol. Opt. Phys. **50**, 182001 (2017).
[11] A. G. Sanz, M. C. Fuss, A. Muñoz, F. Blanco, P. Limão-Vieira, M. J. Brunger, S. J. Buckman, and G. García, Int. J. Radiat. Biol. **88**, 71 (2012).
[12] P. Palihawadana, R. Boadle, L. Chiari, E. K. Anderson, J. R. Machacek, M. J. Brunger, S. J. Buckman, and J. P. Sullivan, Phys. Rev. A **88**, 012717 (2013).
[13] See http://cccbdb.nist.gov/.
[14] C. Hättig, O. Christiansen, S. Coriani, and P. Jørgensen, J. Chem. Phys. **109**, 9237 (1998).
[15] G. Blackman, R. Brown, and F. Burden, J. Mol. Spectrosc. **35**, 444 (1970).
[16] G. M. Moreira and M. H. F. Bettega, J. Phys. Chem. A **123**, 9132 (2019).
[17] J. S. E. Germano and M. A. P. Lima, Phys. Rev. A **47**, 3976 (1993).
[18] C. Winstead and V. McKoy, Phys. Rev. Lett. **98**, 113201 (2007).
[19] C. Winstead and V. McKoy, Phys. Rev. A **76**, 012712 (2007).
[20] J. Tennyson, Phys. Rep. **491**, 29 (2010).
[21] Z. Mašín and J. D. Gorfinkiel, J. Chem. Phys. **135**, 144308 (2011).
[22] P. Palihawadana, J. P. Sullivan, S. J. Buckman, and M. J. Brunger, J. Chem. Phys. **137**, 204307 (2012).
[23] A. G. Sanz, M. C. Fuss, F. Blanco, J. D. Gorfinkiel, D. Almeida, F. F. da Silva, P. Limão-Vieira, M. J. Brunger, and G. García, J. Chem. Phys. **139**, 184310 (2013).
[24] M. C. Fuss, A. G. Sanz, F. Blanco, J. C. Oller, P. Limão-Vieira, M. J. Brunger, and G. García, Phys. Rev. A **88**, 042702 (2013).
[25] J. P. Sullivan, A. Jones, P. Caradonna, C. Makochekanwa, and S. J. Buckman, Rev. Sci. Instrum. **79**, 113105 (2008).
[26] J. P. Sullivan, S. J. Gilbert, J. P. Marler, R. G. Greaves, S. J. Buckman, and C. M. Surko, Phys. Rev. A **66**, 042708 (2002).
[27] J. P. Sullivan, C. Makochekanwa, A. Jones, P. Caradonna, D. S. Slaughter, J. Machacek, R. P. McEachran, D. W. Mueller, and S. J. Buckman, J. Phys. B: At. Mol. Opt. Phys. **44**, 035201 (2011).
[28] Z. Cheong, G. M. Moreira, M. H. F. Bettega, F. Blanco, G. Garcia, M. J. Brunger, R. D. White, and J. P. Sullivan, J. Chem. Phys. **153**, 244303 (2020).
[29] D. Stevens, T. J. Babij, J. R. Machacek, S. J. Buckman, M. J. Brunger, R. D. White, G. García, F. Blanco, L. Ellis-Gibbings, and J. P. Sullivan, J. Chem. Phys. **148**, 144308 (2018).
[30] F. Blanco and G. García, Phys. Rev. A **67**, 022701 (2003).
[31] F. Blanco, L. Ellis-Gibbings, and G. García, Chem. Phys. Lett. **645**, 71 (2016).
[32] F. Blanco and G. García, Phys. Lett. A **317**, 458 (2003).
[33] Z. Mašín, J. Benda, J. D. Gorfinkiel, A. G. Harvey, and J. Tennyson, Comput. Phys. Commun. **249**, 107092 (2020).
[34] J. Franz, F. A. Gianturco, K. L. Baluja, J. Tennyson, R. Carey, R. Montuoro, R. R. Lucchese, T. Stoecklin, P. Nicholas, and T. L. Gibson, Nucl. Instrum. Methods Phys. Res. B **266**, 425 (2008).
[35] R. Zhang, P. G. Galiatsatos, and J. Tennyson, J. Phys. B: At. Mol. Opt. Phys. **44**, 195203 (2011).
[36] J. M. Carr, P. G. Galiatsatos, J. D. Gorfinkiel, A. G. Harvey, M. A. Lysaght, D. Madden, Z. Mašín, M. Plummer, J. Tennyson, and H. N. Varambhia, Eur. Phys. J. D **66**, 58 (2012).

[37] Z. Mašín, *DCS: A Program to Generate Orientation-averaged DCS for Electronically Elastic and Inelastic Collisions*, 2018, https://gitlab.com/Masin/DCS.

[38] M. A. Morrison, Phys. Rev. A **25**, 1445 (1982).

[39] J. P. Sullivan, S. J. Gilbert, and C. M. Surko, Phys. Rev. Lett. **86**, 1494 (2001).

[40] J. P. Sullivan, J. P. Marler, S. J. Gilbert, S. J. Buckman, and C. M. Surko, Phys. Rev. Lett. **87**, 073201 (2001).

[41] P. Caradonna, J. P. Sullivan, A. Jones, C. Makochekanwa, D. Slaughter, D. W. Mueller, and S. J. Buckman, Phys. Rev. A **80**, 060701(R) (2009).

[42] W. R. Wadt, W. A. Goddard III, and T. H. Dunning, J. Chem. Phys. **65**, 438 (1976).